Synergistic Computational and Experimental Design of Covalent Organic Frameworks for Efficient Alcohol Dehydration

Krishna M. Gupta[a,b]*, Srinivasulu Aitipamula, Xavier Chin, and Pui Shan Chow

[a]*Institute of Sustainability for Chemicals, Energy and Environment (ISCE2), Agency for Science, Technology and Research (A*STAR), 1 Pesek Road, Jurong Island, Singapore 627833, Republic of Singapore*

[b]*Department of Chemical Engineering, Indian Institute of Technology, Jammu 181221, J&K, India*

ABSTRACT: Covalent organic frameworks (COFs), a promising class of nanoporous materials, have received significant attention in membrane separation. Currently, several COFs are reported for alcohol dehydration, but they are not efficient owing to pervasive challenge to separate small-sized molecular mixture. Herein, first we have computationally explored a series of COFs with different functionality and aperture size as pervaporation (PV) membrane and identified a novel COF for efficient dehydration of water/alcohol mixtures (90 wt% IPA, 90 wt% n-butanol and 90 wt% t-butanol). Subsequently, the best performing COF was experimentally synthesized, characterized, and its sorption properties were correlated with computational results. Molecular dynamics (MD) simulations revealed that solvent permeation fluxes are predominantly influenced by the pore aperture of COFs, larger pore aperture exhibits higher flux. Conversely, separation factor is primarily determined by the polarity of the pore functional groups. Among the tested COF membranes, TpPa-1-OC3H6OCH3 demonstrated superior performance, surpassing the current state-of-the-art membranes. Activation energy (Ea) for water permeation in alcohol mixtures through TpPa-1-OC3H6OCH3 is mostly governed by water-alcohol interactions. Furthermore, experimental evaluation of the COFs indicated a plate like morphology for TpPa-1-OC3H6OCH3 which ascertained 2D sheet like structure. TpPa-1 showed greater sorption than TpPa-1-OC3H6OCH3 with all the solvents tested owing to the inability of the solvent molecules to enter the relatively small pores in the later COF. This is in accord with the MD simulation predictions, which indicated that the solvent molecules cannot penetrate the small pores of TpPa-1-OC3H6OCH3. This work synergistically integrates computational and experimental approaches to develop novel COFs with superior performance compared to previously reported PV membranes, paving the way for the advanced membranes for sustainable solvent recovery.

Keywords: membrane separation, COF, molecular simulation, alcohol dehydration, solvent recovery, sustainability

1. INTRODUCTION

Organic solvents play an integral part of chemical processes as raw materials, reaction media, recrystallizing media and cleaning agents.[1] Though the solvents are extensively used in various industries, their recovery and reuse have only gained significant attention recently due to stringent regulatory requirements at reducing the use of toxic solvents and promoting environmentally friendly, sustainable chemical processes.[2, 3] Notably, extensive research has focused on removing water (dehydration) from water/alcohol mixtures. This stems from the fact that alcohol is considered as a major source of energy and currently utilized in the production of biofuel, rocket fuel and medical sanitizer.[4-6] Water and alcohol form an azeotropic mixture, and while distillation is the most used technique for their separation, it is often energy intensive. Pervaporation (PV) has recently emerged as a method of choice for water/alcohol separation (alcohol dehydration). The technique is highly regarded for its cost-effectiveness, energy efficiency, and demonstrated applications in separating azeotropic mixtures.[6-9]

PV uses a porous membrane that selectively enables passage of solvents of smaller dimensions and facilitate separation of solvents from their mixtures. The effectiveness of PV primarily depends on the type of membrane employed.[7] Several membrane materials have been tested for water/alcohol separation including polymeric membrane, mixed matrix membranes, and inorganic membranes (zeolites and silica-based).[10-12] These membranes are susceptible to several drawbacks such as physical deterioration, inconsistencies during long-term operations, difficulties in fabricating defect-free membranes, etc. [13, 14] As pore size is the determining factor for the separation of solvents using the PV membrane, last decade has witnessed a significant paradigm shift towards development of novel materials for separating organic solvents.

Covalent organic frameworks (COFs) have received a significant traction due to their tuneable pore size, customizable polarity, and ease of synthesis.[15, 16] Recently, several COFs have been found promising for dehydration of alcohols. For example, Yang et al. synthesized a series of COF

membranes through a mixed-dimensional assembly of COF nanosheets and cellulose nanofibers and achieved a separation factor of 3876 for *n*-butanol dehydration.[17] Similarly, a robust and stable functionally-graded COF membranes for ethanol dehydration was prepared that showed separation factor two times higher than that of commercial membranes.[18] For *n*-butanol dehydration, Zhang et al. synthesised TpHZ/PAN COF membranes that conferred numerous hydrophilic pathways for water-selective transport, exhibited a high and stable dehydration performance with permeation flux of 8160 $kg/m^2.h^{-1}$ and separation factor of 1023.[19] Wang et al. fabricated a keto-enamine-linked COF (TpPa-1) on commercial polyacrylonitrile (PAN) through an oxygen-plasma assisted contra-diffusion self-assembly strategy. Defect-free TpPa membrane exhibited a separation factor of 1491 and a high permeation flux of 2.53 $kg/m^2.h^{-1}$ for isopropanol (IPA) dehydration.[20] Jin and co-workers recently reported a hybrid membrane using TpPa-1 to enhance dehydration performance of water/butanol mixtures. Dehydration performance demonstrated significant improvements in total flux and separation factor when TpPa-1 nanosheets and sodium alginate (SA) were integrated.[21]

Although above studies demonstrate promising results, there remains a need to develop novel COFs with enhanced separation performance by further reducing the pore size.[22] One of the key strategies in membrane design is understanding the role of pore size and membrane polarity.[6, 23,24] Pore size determines the trade-off between permeation and selectivity; specifically, larger pores increase permeation but lower selectivity, while smaller pores enhance selectivity but reduce permeation. In terms of polarity, hydrophilic membranes are ideal for aqueous separations, as they resist fouling from organic contaminants. In contrast, hydrophobic membranes are primarily used for organic solvent filtration. Additionally, polarity influences how different solutes/solvents adsorb onto the membrane, affecting fouling behaviour and long-term performance. Therefore, in our previous work, using TpPa-1 (derived from 1,3,5-triformylphloroglucinol (Tp) and *p*-phenylenediamine (Pa-1)) as the model parent structure, we computationally designed novel COFs with varying pore size via grafting polar and nonpolar linkers on the TpPa-1 backbone. Subsequently, evaluation of their ability to separate

water-ethanol mixtures by molecular dynamics (MD) simulations revealed not only the pore size, but also the hydrophilic pore functionality plays a critical role in determining the separation performance. For example, functionalizing the TpPa-1 backbone with a -C4H8OH group resulted in the COF, TpPa-1-C4H8OH, which exhibited an optimal pore size and hydrophilicity for efficient ethanol dehydration.[25] Motivated by this initial finding, we have now expanded our research to study the dehydration of other alcohols (IPA, *n*-butanol and *t*-butanol) using the previously designed COFs and a novel COF, TpPa-1-OC3H6OCH3, by MD simulation. The parent and new COFs were also experimentally synthesized and its ability to adsorb the solvents was evaluated and correlated with computationally derived PV results.

2. MATERIALS AND METHODS

2.1. Computational methodology

When selecting a COF for solvent recovery, it is essential to consider its structural robustness, including thermal, chemical, and hydrothermal stability, as well as its resistance to common organic solvents. Furthermore, the COF should have a moderate pore size, amenable to structural modification, and feasible to synthesize using traditional experimental approaches. We have chosen TpPa-1 as the COF of interest due to its good chemical and hydrothermal stability.[26] Additionally, prior to computational modifications, we ensured that the computationally designed COFs could be synthesized using traditional experimental approaches. The parent COF (TpPa-1) is not suitable for alcohol dehydration as the aperture diameter (da) is around 15.6 Å which is larger than the molecular size of the targeted solvents (Figure 1). Therefore, to enhance the dehydration performance, we strategically reduced the d_a of TpPa-1 by grafting functional groups on its framework. Precisely, five COFs have been computationally designed namely TpPa-1-C5H8, TpPa-1-COOC2H5, TpPa-1-OC3H6OH, TpPa-1-C2Ph, and TpPa-1-OC3H6OCH3 (**Figure 1**) via grafting polar and nonpolar linkers.

These COFs are expected to confer a greater degree of variation in the pore size and affinity towards solvent molecules, thus expected to improve the separation performance. COF structures were initially constructed in Materials Studio (Version 2020)[27] and were symmetrically optimised using density functional theory calculations performed with the Vienna Ab Initio Simulation Package (VASP).[28-31] Using optimised structures, d_a values were estimated. The d_a is defined as the size of the largest sphere that can pass through the aperture without touching any framework atoms. This value is determined using the Zeo++ software.[32] The d_a of the designed COFs are smaller than that of the parent COF (TaPa-1) and increases in the order of TpPa-1-OC3H6OCH3 < TpPa-1-C2Ph < TpPa-1-OC3H6OH < TpPa-1-COOC2H5 < TpPa-1-C5H8.

PV has been widely implemented for liquid phase separation including alcohol dehydration,[6-9] therefore, the designed COFs were tested as PV membranes to gauge the dehydration performance. To mimic PV separation close to the realistic scenario, we have adopted our recently developed PV simulation protocol.[33] As illustrated in **Figure 2**, simulation model contains a feed chamber (left), a COF membrane and a permeate chamber (right). Similar to our recent work,[25] for each COF, first a 2 × 3 supercell was generated using a unit cell of the designed COF which results in a dimension of ~7.7 Å × 6.7 Å in the *x* and *y* directions. Then, using this COF sheet, 6 COF sheets were generated to use as a COF membrane in PV simulation. **Figure S1** of the supporting information show the supercell and 6-layer structure of a novel designed COF. Feed chamber contains a solution with 10 wt% water and 90 wt% alcohol (IPA or *n*-butanol or *t*-butanol) and a vacuum which facilitates the evaporation of the feed solution, allowing it to coexist with a vapor phase (VLE) during simulation. The right chamber comprises a vacuum. The graphene plates serve as reflective walls and have minimal interaction with any matter. Once the molecules pass through the COF membrane from the left chamber to the right chamber, they are periodically extracted. By undergoing this process, the permeate side experiences decreased pressure, which establishes a consistent driving force between the chambers on the left and right, thus facilitating the vaporization and subsequent permeation of the solvent.

The Lennard-Jones (LJ) and electrostatic potentials were used to mimic the atomic interactions in the COF frameworks as:

$$\sum 4\varepsilon_{ij}\left[\left(\frac{\sigma_{ij}}{r_{ij}}\right)^{12}-\left(\frac{\sigma_{ij}}{r_{ij}}\right)^{6}\right]+\sum\frac{q_i q_j}{4\pi\varepsilon_0 r_{ij}} \quad (1)$$

where ε_{ij} and σ_{ij} are the well depth and collision diameter, r_{ij} is the distance between atoms i and j, q_i is the atomic charge of atom i, and $\varepsilon_0 = 8.8542 \times 10^{-12}$ $C^2N^{-1}m^{-2}$ is the permittivity of vacuum. To estimate the atomic charges on the atoms of the COFs, the Density-Derived Electrostatic and Chemical (DDEC) method,[34] which relies on density functional theory calculations performed with the Vienna Ab Initio Simulation Package (VASP)[28-31] was utilized. The projector augmented wave formalism-based potentials were adopted. For all the calculations, a cut-off value of 400 eV was used for the plane-wave basis set. The Monkhorst–Pack *k*-point grid of size 1×1×5 was applied for both vacancy and bulk supercell total energy calculations. The generalized gradient approximation (GGA) exchange–correlation functionals, which account for both electron density and its gradient in the exchange-correlation functional, were utilized. The estimated atomic charges of newly designed COF is shown in **Figures S2** of the supporting information, whereas for other COFs were reported in our recent work.[25]

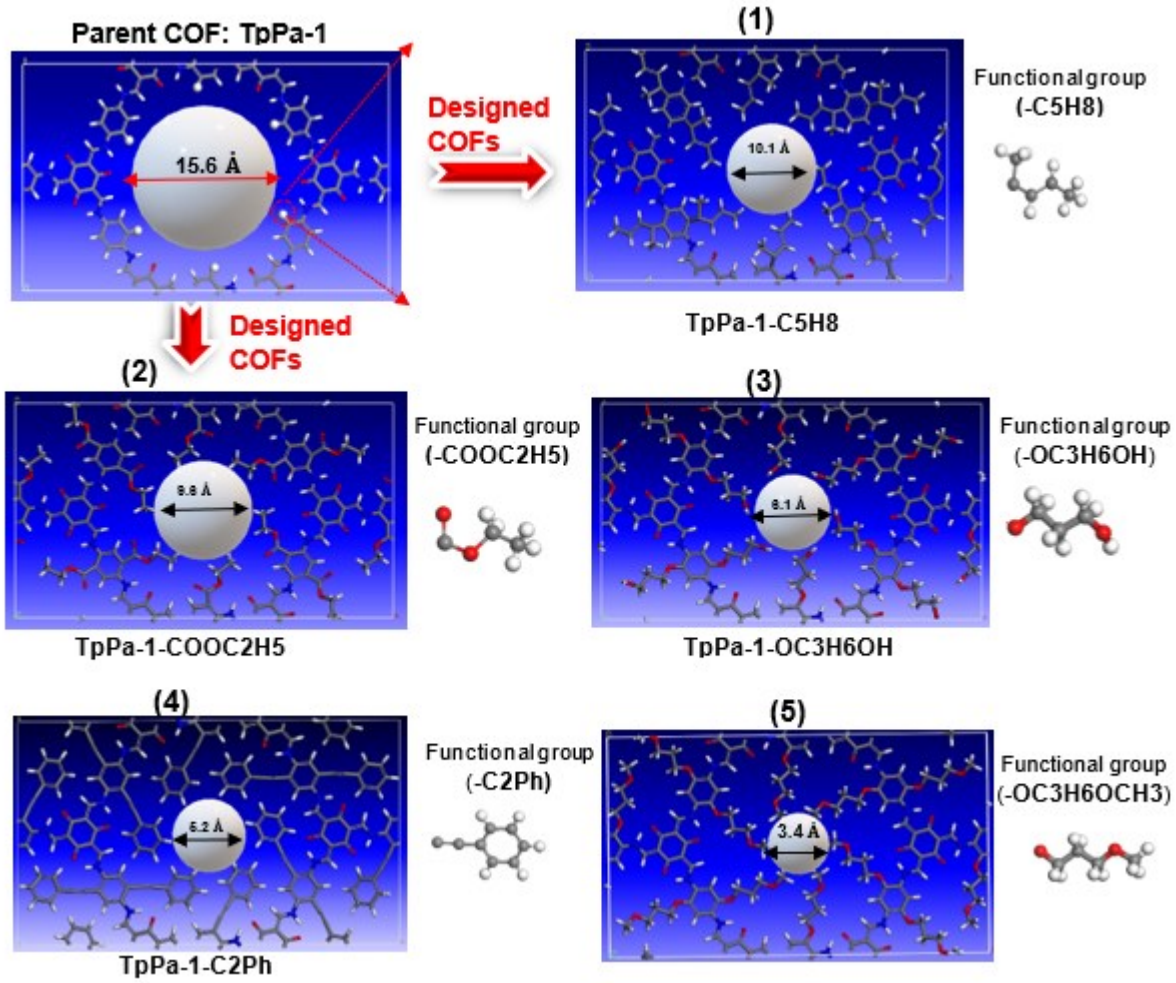

Fig. 1. Structures of computationally designed COFs. The predicted pore sizes are shown in white spheres.

As illustrated in **Table S1** of the supporting information, the LJ parameters were taken from the Universal Force Field (UFF).[35] During simulations, COF structures were kept rigid as nanoporous membrane simulations involving rigid structures offer a reliable, precise, and accurate prediction.[33] It has potentially been applied not only for COF simulation[25, 36] but also to various other porous membrane simulations, including nanoporous graphene[37], porous organic cages[38], and graphene oxide[39]. The parameters for alcohols (IPA, *n*-butanol and *t*-butanol) were defined using the Optimized Potentials for Liquid Simulations all-atom (OPLS-AA) force field[40] as this force field is able to effectively mimic solvent model in simulation.[41] The parameter files were first generated using the MKTOP tool[42] and then atomic charges were corrected according to OPLS-AA force field. The water was modelled by the TIP3P.[43] The carbon atoms in graphene plates were characterized by reducing

the Lennard-Jones (LJ) parameters in the absence of charge, which act as reflective boundaries with minimal interaction with any species.

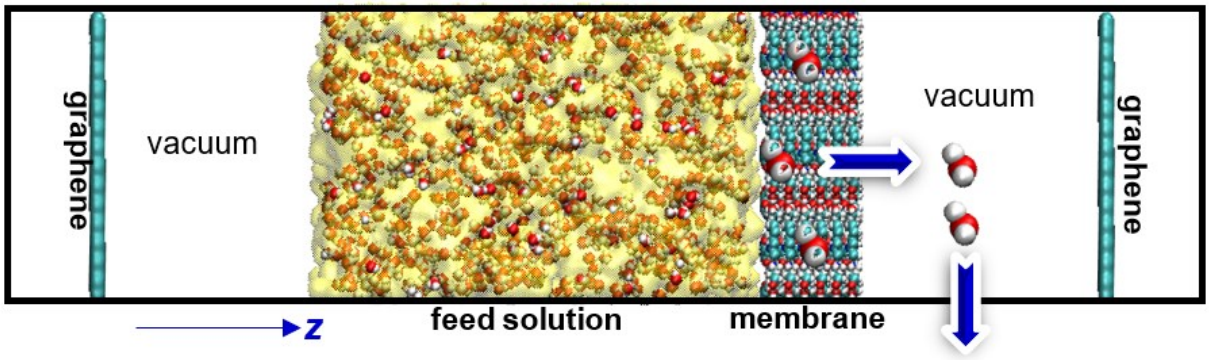

Fig. 2. A schematic representation of PV simulation system. The left chamber contains feed solution (10 wt% water and 90 wt% alcohol), a vacuum and a graphene plate. The right chamber contains a vacuum (permeated molecules through the membrane are removed periodically) and a graphene plate. Colour code: alcohol, yellow surf; H, white; C, cyan; O, red.

Prior to MD simulations, the systems underwent energy minimization utilizing the steepest descent method with a maximum step size of 0.1 Å and a force tolerance of 1 kJ/(mol·Å). Subsequently, velocities were assigned to the systems, and MD simulations were conducted in the canonical ensemble. The temperature was maintained at 80 °C (353 K). The velocity rescaling thermostat was used with a relaxation time of 0.1 ps to control the temperature. The LJ interactions were computed using a 14 Å cut-off, while the electrostatic interactions were evaluated employing the particle-mesh Ewald method with a grid spacing of 1.2 Å and a real-space cut-off of 14 Å. The equations of motion were solved using the leapfrog algorithm with a time step of 1 fs. The molecular flux is influenced by the d_a of COF membrane. Therefore, to sustain the extremely low pressure on the permeate side and achieve adequate molecular permeation, both simulation time and removal interval were controlled. Particularly, in all feed mixtures, simulation duration and removal interval were 5 ns and 1 ps, respectively, for TpPa-1 and TpPa-1-C5H8 due to the larger d_a (fast permeation). With moderate d_a of TpPa-1-COOC2H5 and TpPa-1-OC3H6OH, simulation duration and removal interval were 20 ns and 10 ps, respectively. With smaller d_a, simulation duration and removal interval were 50 ns and 10 ps, respectively for TpPa-1-C2Ph and TpPa-1-OC3H6OCH3. To estimate the E_a of water through the top-

performing membrane, additional simulations were conducted at 320 and 340 K with each simulation duration of 50 ns, corresponding to all three mixtures. Simulations were conducted using the GROMACS v2016.3 package.[44]

2.2. Experimental

2.2.1. Materials

Tp was purchased from Alfachem, China, Pa-1, *p*-toluenesulfonic acid, *n*-butanol, *t*-butanol were purchased from Sigma Aldrich, Singapore, 1,4-dioxane and acetone were purchased from Merck, Singapore, mesitylene was purchased from Acros Organics, Thermo Fischer, Singapore, dimethylformamide and acetic acid were purchased from VWR Chemicals, Singapore, and TpPa-1-OC3H6OCH3 was synthesized in collaboration with NSJ Prayog Lifesciences Pvt Ltd., Hyderabad, India. Ultrapure water was used for purification of the COF powders.

2.2.2. Synthesis of COFs. TpPa-1 and TpPa-1-OC3H6OCH3 were synthesized by acid-catalyzed condensation reaction using Tp and the corresponding 1,4-diamine ligand (**Scheme 1**).

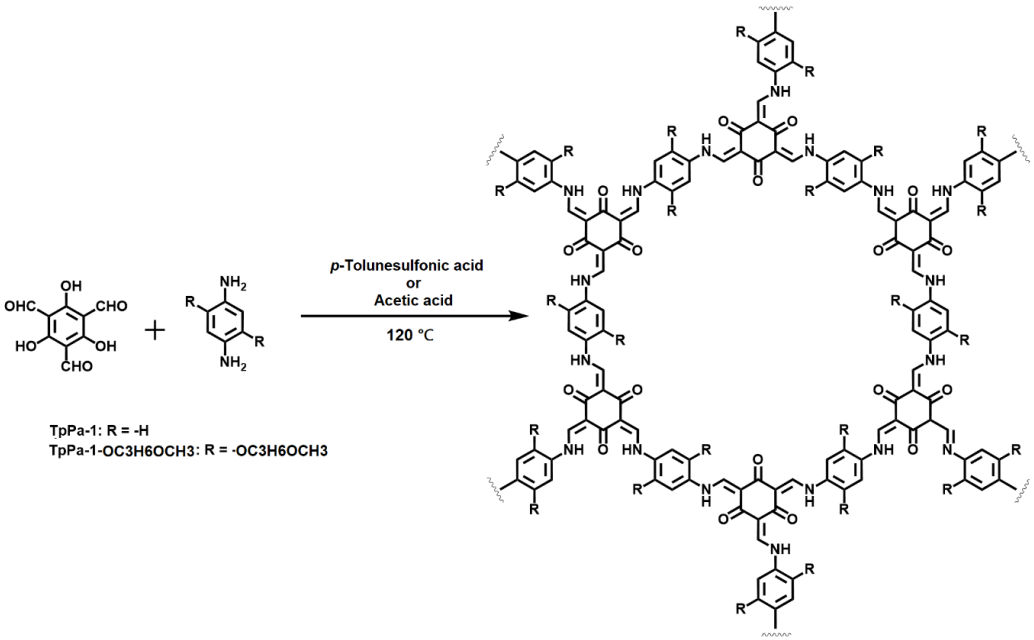

Scheme 1. A general scheme for the synthesis of TpPa-1 and TpPa-1-OC3H6OCH3.

TpPa-1*:* A synthesis protocol reported previously was adopted for the synthesis of TpPa-1.[45] In a typical experiment, the building blocks of the COF, namely, Tp (63 mg, 0.3 mmol) and Pa-1 (48 mg, 0.45 mmol) were placed in a pyrex tube (o.d. × i.d. = 10 × 8 mm^2 and length 18 cm) and 1.5 mL of mesitylene and 1.5 mL of 1,4-dioxane were added. *p*-toluene sulfonic acid (58 mmol, 10 g) (0.5 mL) was used as a catalyst. The reaction mixture was sonicated for 10 minutes for thorough mixing of the ingredients. Subsequently, the pyrex tube was sealed with a cap and kept at 120 °C for 3 days in an oven. Color of the reaction solids gradually turned red as the reaction proceed to completion. The dispersion was filtered using a vacuum pump and the precipitate was washed with a copious amount of acetone and water. The resulting powder was heated to 120 °C and dried in an oven for 24 hours to give the TpPa-1 in 75 % (89 mg) yield. IR (powder, cm^{-1}): 1584 (s), 1516 (s), 1457 (s), 1274 (s), 1159 (m), 1034 (s), 1009 (s), 816 (s), 682 (s).

TpPa-1-OC3H6OCH3*:* Synthesis of TpPa-1-OC3H6OCH3 was developed in collaboration with NSJ Prayog Life Sciences Pvt Ltd., Hyderabad, India,[46] which involved multi-step synthesis of 1,4-diamine ligand followed by condensation with Tp to obtain the desired Schiff base (**Scheme 2**).

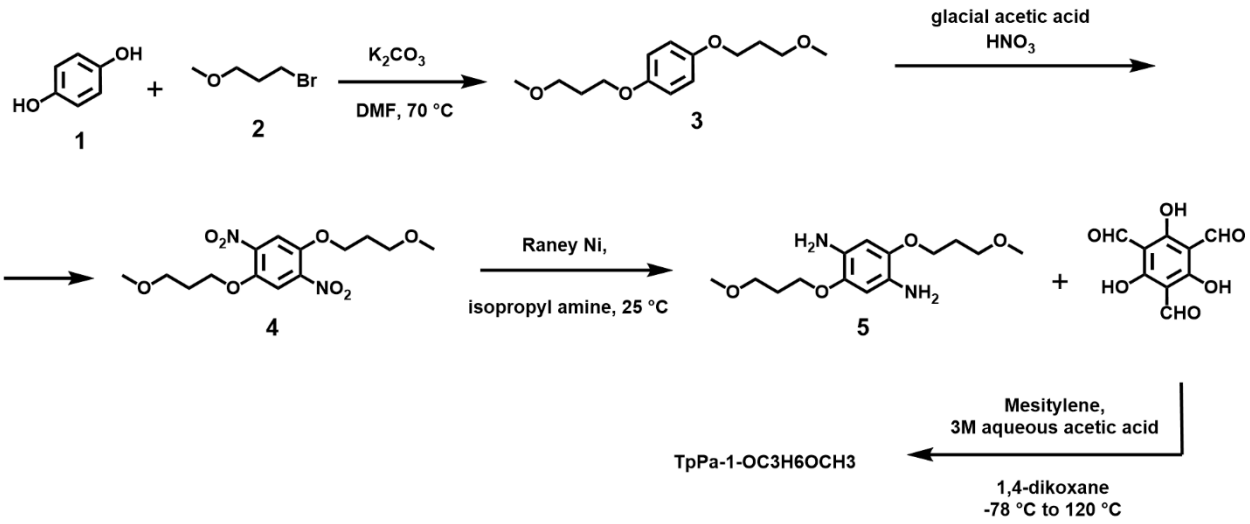

Scheme 2. Schematic representation of the synthesis of TpPa-1-OC3H6OCH3.

Synthesis of 1,4-bis(3-methoxypropoxy)benzene (**3**). Hydroquinone **1** (10.0 g, 90.0 mmol, 1.0 eq.), potassium carbonate (62.7 g, 454 mmol, 5.0 eq.), and 1-bromo-3-methoxypropane **2** (41.7 g, 272 mmol, 3.0 eq.) were dissolved in 100 mL of DMF and stirred at 70 ℃ for 24 h under nitrogen atmosphere. The reaction mixture was subsequently filtered, added cold water to the filtrate, and extracted with ethyl acetate (100 mL x 3). The organic layer was washed multiple times with cold water and dried over anhydrous Na_2SO_4 and concentrated under vacuum. Purification by column chromatography afforded compound **3** as white semi solid (15.0 g, 65%). ^{1}H NMR (400 MHz, Chloroform-*d*): δ 6.83 (s, 4H), 4.00 (t, J = 6.3 Hz, 4H), 3.55 (t, J = 6.2 Hz, 4H), 3.35 (s, 6H), 2.02 (t, J = 6.3 Hz, 4H).

Synthesis of 1,4-bis(3-methoxypropoxy)-2,5-dinitrobenzene (**4**). Compound **3** (15.0 g, 59.1 mmol, 1.0 eq.) was dissolved in 50 mL of glacial acetic acid. To this solution, 18 mL of 37% nitric acid was added and stirred for 1–2 hours. The resulting reaction mixture was subsequently diluted with water (50 mL) and neutralized with aqueous KOH. Upon extracting with ethyl acetate, the combined organic layers were dried using Na_2SO_4 and concentrated under vacuum. Purification by column chromatography afforded compound **4** as a yellow solid (4.5 g, 20%). ^{1}H NMR (400 MHz, Chloroform-*d*) δ 7.56 (s, 2H), 4.21 (t, J = 6.1 Hz, 4H), 3.56 (t, J = 5.9 Hz, 4H), 3.35 (s, 6H), 2.09 (p, J = 6.0 Hz, 4H).

Synthesis of 2,5-bis(3-methoxypropoxy)benzene-1,4-diamine (**5**). Compound **4** (4.50 g, 13.1 mmol, 1.0 eq.) was dissolved in isopropyl amine (45 mL) and stirred. To this solution, Raney Ni (20.0 g, 265 mmol, 20 eq.) was added and stirred overnight at 25 °C. The mixture was subsequently filtered, and the residue was washed with isopropyl amine. Compound **5** was obtained as a brown solid upon removing the organic solvent by a rotary evaporator. Yield: 2.50 g (75%). ^{1}H NMR (400 MHz, DMSO-*d*6) δ 6.27 (s, 2H), 3.94 (s, 4H), 3.83 (t, J = 6.3 Hz, 4H), 3.47 (t, J = 6.3 Hz, 4H), 3.24 (s, 6H), 1.90 (t, J = 6.3 Hz, 4H); ESI *m/z*: 285.2 [M + H]+.

Synthesis of TpPa-1-OC3H6OCH3. A sealed tube was charged with compound **5** (2.50 g, 8.80 mmol, 1.0 eq.), Tp (1.80 g, 5.28 mmol, 0.6 eq.), mesitylene, (60 mL), 3M aqueous acetic acid (20 mL), and 1,4-dioxane (60 mL) and sonicated for 10 min to achieve a homogeneous dispersion. The tube was then frozen at -78 °C using a dry ice bath and degassed via freeze-pump-thaw cycles. The sealed tube was heated at 120 °C for 3 days. TpPa-1-OC3H6OCH3, which was formed as red precipitate, was filtered under vacuum and washed copious amounts of anhydrous acetone. Subsequently, the COF powder was solvent-exchanged with anhydrous acetone 5–6 times and then dried at 180 °C under vacuum for 24 hours yielding a deep red powder (3.20 g). IR (KBr): 1575, 1437, 1249, 1115, 837 cm-[1]. Anal. Calcld. For C60O18N6H72: C, 61.8; H, 6.2; N, 7.2; found: C, 58.6; H, 5.7; N, 6.6.

2.2.3. Characterization. *Powder X-ray diffraction (PXRD):* Crystallinity of the bulk powders of TpPa-1 and TpPa-1-OC3H6OCH3 was analyzed by D8 Advance powder X-ray diffractometer (Bruker AXS GmbH, Germany) with Cu-Kα radiation (λ = 1.54056 Å). The diffractions was operated at a voltage of 35 kV and current of 40 mA. Samples were scanned in the range of 2θ = 1° to 50° at a scan rate of 5 deg min^{-1}.

Spectroscopy: PerkinElmer spectrum 100 FT-IR Spectrophotometer (ATR) was used for the characterization of the COF powders. The samples were analyzed in transmittance mode between the 4000-400 cm^{-1} in 64 scans.

Dynamic vapour sorption (DVS): Water vapor sorption isotherms were measured using a Surface Measurement Systems Advantage dynamic vapour sorption (DVS) instrument at 25 °C. Approximately 10 mg of COF powders were exposed to a relative humidity range of 0% to 90% in 9 steps, followed by desorption. Samples were equilibrated until the mass change rate was less than 0.002% min^{-1}, after being dried for 6 hours at 25 °C and 0% vapor pressure. Similarly, sorption and desorption isotherms using IPA, *t*-butanol, and *n*-butanol were determined by replacing the water with the corresponding solvents.

Elemental analysis: Thermo Fisher Scientific FLASH 2000 CHNS/O Analyzer was used for quantification of carbon, nitrogen, and oxygen present COF samples.

***Brunauer-Emmett-Teller (BET) isotherms*:** The N_2 physisorption was measured at -196 °C on a static volumetric equipment Micromeritics ASAP 2420MP instrument. The dry COF powders were degassed in a vacuum oven at 100 °C for 24 h before the measurements. The specific surface area, total pore volume, and average pore diameter of samples were established from the N_2 isotherms using the BET method.

Scanning Electron Microscopy (SEM): Scanning electron microscope (SEM, JEOL, JSM-7610F, Tokyo, Japan) was used for analysing the morphology of the COF powders. The microscope was operated at 1.5 kV. The samples were prepared by drop-casting the diluted dispersion of COF powders on a silicon wafer and were coated with a thin layer of gold prior to analysis.

3. RESULTS AND DISCUSSION

3.1 Permeation flux and separation factor

Usually, performance of a membrane is evaluated by flux and separation factor, therefore we have adopted these two matrices to gauge the performance of the COF membranes. Once the simulation was initiated, water and alcohol molecules from the left chamber (feed) entered the membrane and subsequently passed into the right chamber (permeate). Over time, the number of water or alcohol molecules in the permeate chamber increased, indicating the PV process. The flow rates of water and alcohol through the COF membranes were calculated. **Figure 3** shows the net water (N_{water}) and IPA (N_{IPA}) transferred with time. The N_{IPA} is higher than N_{water} in TpPa-1, TpPa-1-C5H8, TpPa-1-COOC2H5, and TpPa-1-C2Ph. This phenomenon could be attributed to two key factors: 1) the higher concentration of IPA, i.e. greater availability of IPA molecules enhances their ability to pass through the membrane more readily, 2) the pores of these membranes exhibit hydrophobic characteristics,

which promote favourable interactions with IPA molecules and enable higher number of IPA molecules to pass through the membrane. Consequently, these two factors work in tandem to result in increased IPA transport through the membrane. In contrast, having a hydrophilic pore characteristic, TpPa-1-OC3H6OH shows higher N_{water} than N_{IPA} even though the feed solution contains higher IPA concentration.

Figure 4 & **Figure 5** show the net water (N_{water}) and *n*-butanol ($N_{n\text{-butanol}}$) as well as N_{water} and *t*-butanol ($N_{t\text{-butanol}}$) transferred with time. Like water-IPA mixture, both $N_{n\text{-butanol}}$ and $N_{t\text{-butanol}}$ are higher than N_{water} in TpPa-1, TpPa-1-C5H8, TpPa-1-COOC2H5, and TpPa-1-C2Ph due to both higher concentration of these alcohols and hydrophobic pore characteristics of these COFs that creates favourable interactions for alcohol molecules to pass through the pores. Higher flow of alcohol compared to water from water/alcohol mixture through the hydrophobic frameworks, particularly GME zeolitic–imidazolate, MFI zeolite and COF framework membranes, has also been observed previously.[25, 33, 47] The N_{water} is higher or close the $N_{n\text{-butanol}}$ and $N_{t\text{-butanol}}$, even though the feed solution contains higher alcohol concentration owing to hydrophilic pore characteristic of TpPa-1-OC3H6OH. This is consistent with our previous work where the higher flow of water over ethanol for water/ethanol mixture through hydrophilic COF membranes was observed.[25] In the case of TpPa-1-C2Ph, the permeation of water and *t*-butanol is extremely low compared to other COFs. Strong interaction of *t*-butanol with TpPa-1-C2Ph framework atoms restricts the permeation and hence restricted motion of *t*-butanol creates hindrance for water to pass through the pores, showing extremely low permeation of water and *t*-butanol. Interestingly, due to a significantly smaller aperture size (d_a = 3.4 Å), only water flow is seen through TpPa-1-OC3H6OCH3 for all three alcohol mixtures (water/IPA, water/*n*-butanol, and water/*t*-butanol).

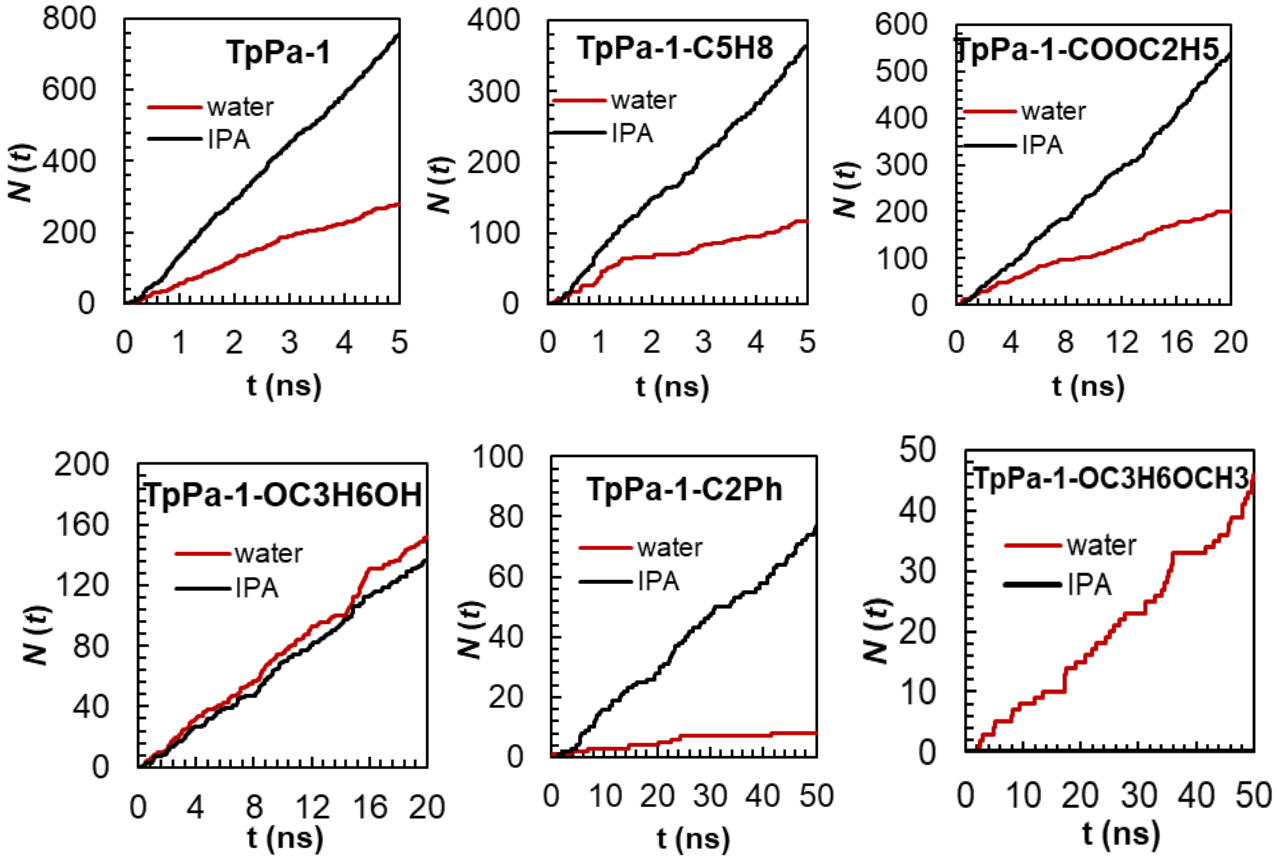

Fig. 3. Net water and IPA transfer with time through COF membranes during PV simulation process.

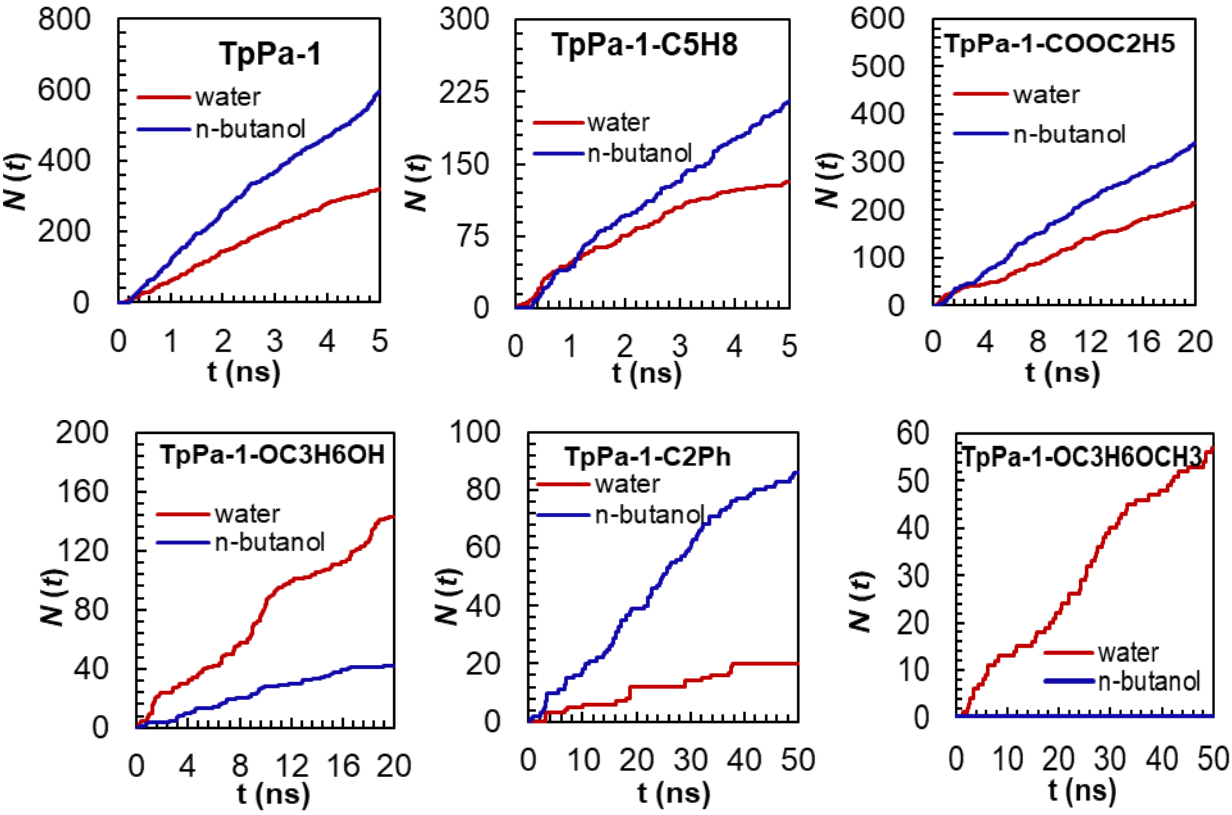

Fig. 4. Net water and *n*-butanol transfer with time through COF membranes during PV simulation process.

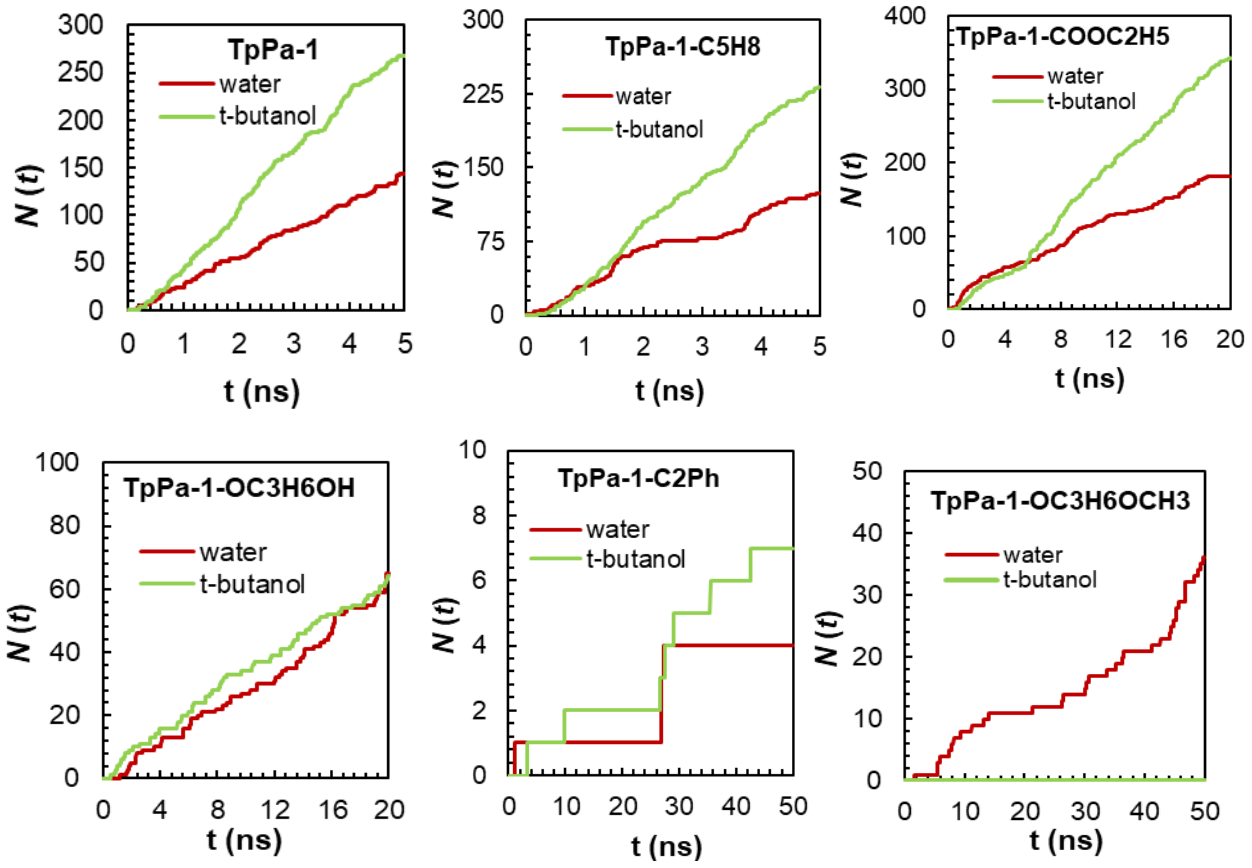

Fig. 5. Net water and *t*-butanol transfer with time through COF membranes during PV simulation process.

As the net flow of water and alcohols through COF membranes increases almost linearly with time, their fluxes were calculated from the slope using $J = N/(A \cdot t)$, where A is the membrane area and t is the time. **Figure 6a** depicts the water (J_w), IPA (J_{IPA}) and total ($J_{t:(IPA)}$) fluxes through the COF membranes for water/IPA mixture. The hierarchy of the fluxes is TpPa-1 > TpPa-1-C5H8 > TpPa-1-COOC2H5 > TpPa-1-OC3H6OH > TpPa-1-C2Ph > TpPa-1-OC3H6OCH3. In general, the permeation flux of a solvent molecule is mostly governed by the d_a. With the largest d_a, TpPa-1 holds the highest flux whereas the smallest d_a leads to the lowest flux in TpPa-1-OC3H6OCH3. Similarly, fluxes for water (J_w), *n*-butanol ($J_{n\text{-butanol}}$) and total ($J_{t(n\text{-butanol})}$) for water/*n*-butanol mixture and water (J_w), *t*-butanol ($J_{t\text{-butanol}}$) and total ($J_{t(t\text{-butanol})}$) for water/*t*-butanol mixture through COF membranes are shown in **Figure 6b & 6c**. For these mixtures, the trend of permeation fluxes is same as water/IPA mixture,

i.e., the permeation fluxes of water and alcohols are mainly governed by the d_a. The largest d_a leads to the highest flux in TpPa-1, whereas the smallest d_a leads to the lowest flux in TpPa-1-OC3H6OCH3. Due to significantly smaller aperture size, IPA, *n*-butanol and *t*-butanol molecules could not pass through the TpPa-1-OC3H6OCH3 membrane. This phenomenon (i.e., flux primarily governed by the aperture size) has also been reported for water/ethanol separation in COFs[25] and seawater PV through zeolitic imidazolate framework membranes.[48]

Furthermore, the separation factor of water over alcohols is defined as

$$S_{w/a} = \frac{y_{w/y_a}}{x_{w/x_a}} \quad (2)$$

where y_w and x_a are the mass fractions of water and alcohols in the permeate and feed chamber. Consistent with our previous work,[25] mass fractions of water and alcohols in the permeate chamber were calculated using number of these molecules permeated at the end of simulation, whereas mass fractions of water and alcohols in the feed chamber were taken as initial feed concentration, i.e. (10 wt% water and 90 wt% alcohol) at 80 °C. As shown in **Figure 7**, for all water/alcohol mixtures, in contrast to flux, separation factor is not mainly governed by the d_a, instead both polarity of the pores and d_a play a crucial role. For all water/alcohol mixtures, membranes with hydrophobic pore characteristics (TpPa-1-C5H8, TpPa-1-COOC2H5 and TpPa-1-C2Ph) display a lower separation factor than the membrane with hydrophilic pore (TpPa-1-OC3H6OH). As water flow through the small pores or channels in amorphous membranes such as polymeric and carbon membranes (CRNL-(OH)2 and CRNL) is primarily governed by the entry of water into the membrane,[49] water molecules can pass through the small pore aperture in TpPa-1-OC3H6OH, leading to a higher water selectivity. The higher separation factor of water for water/ethanol mixture in hydrophilic COF membranes compared to hydrophobic COF membranes is also found to be primarily governed by favourable entry of water into the membrane.[25] Interestingly, the TpPa-1-OC3H6OCH3 shows 100% retention for alcohols over water. This is attributed to the smaller d_a compared to molecular sizes of alcohols. Precisely, the kinetic diameters of the IPA, *n*-butanol and *t*-butanol are 4.7 Å, 5.0 Å, and 6.0 Å,[50, 51] respectively which are

larger than the d_a (3.4 Å) of newly designed COF (TpPa-1-OC3H6OCH3), thus leading to 100% retention for alcohols over water. Therefore, TpPa-1-OC3H6OCH3 could be a promising candidate for the efficient separation of water from water/alcohol mixtures.

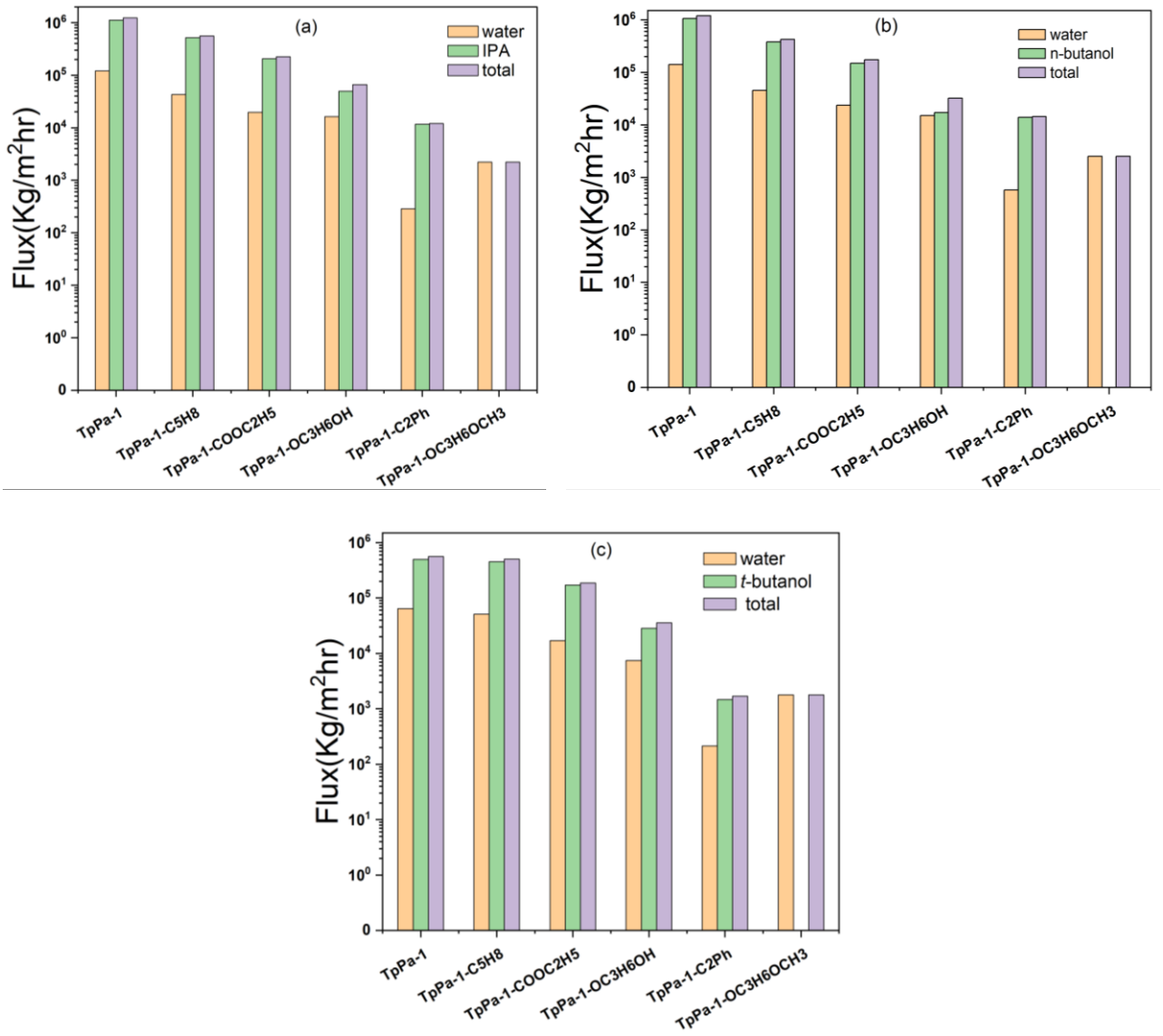

Fig. 6. Flux (J) through the COF membranes for (a) water/IPA (b) water/*n*-butanol and (c) water/*t*-butanol mixtures by MD simulation.

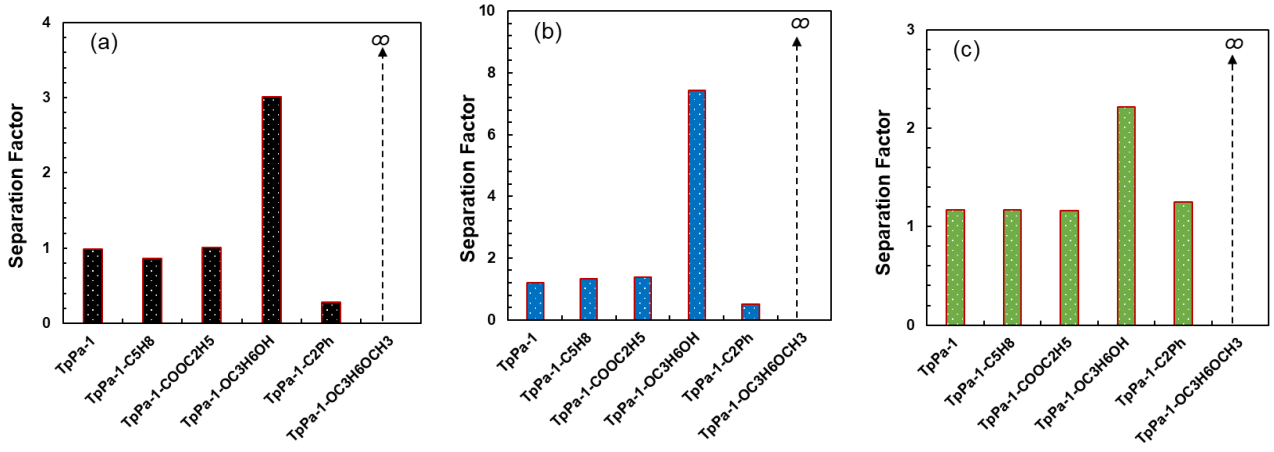

Fig. 7. Separation factors for (a) water/IPA (b) water/*n*-butanol and (c) water/*t*-butanol mixtures by MD simulation.

3.2 Separation Performance

The performance of the newly designed COF membrane (TpPa-1-OC3H6OCH3) against literature reported membranes in terms of their permeation flux and separation factor at similar operating conditions (temperature ranges from 60 to 80 °C, feed mixture: 90 wt% alcohol) were compared in **Figure 8**. Theoretically predicted permeation fluxes through the TpPa-1-OC3H6OCH3 are significantly higher compared to the state-of-the-art membranes for all mixtures such as water/IPA (silica, metal-organic framework, and COF-based membranes)[20, 52], water/*n*-butanol (graphene oxide, metal-organic framework, COF-based membranes),[21, 52, 53] and water/*t*-butanol (PVA, silica, and COF-based membranes).[54, 55] Importantly, for all the three alcohol mixtures, separation factors for the TpPa-1-OC3H6OCH3 membrane show complete retention of alcohol (separation factor $\sim\infty$). Additionally, thickness normalized permeation fluxes through highly selective TpPa-1-OC3H6OCH3 membrane are 4.50, 5.08 and 3.63 kg.μm/m^2.hr for water/IPA, water/*n*-butanol and water/*t*-butanol mixtures, respectively. These are remarkably higher than recently reported COF-based membranes: ~0.8 kg.μm/m^2.hr (water/IPA), 0.66 to 2.11 kg.μm/m^2.hr (water/*n*-butanol), and 1.56 kg.μm/m^2.hr (water/*t*-butanol).[21, 54] Overall, among all the tested membranes, TpPa-1-OC3H6OCH3 membrane shows excellent performance compared to the current state-of-the-art membranes.

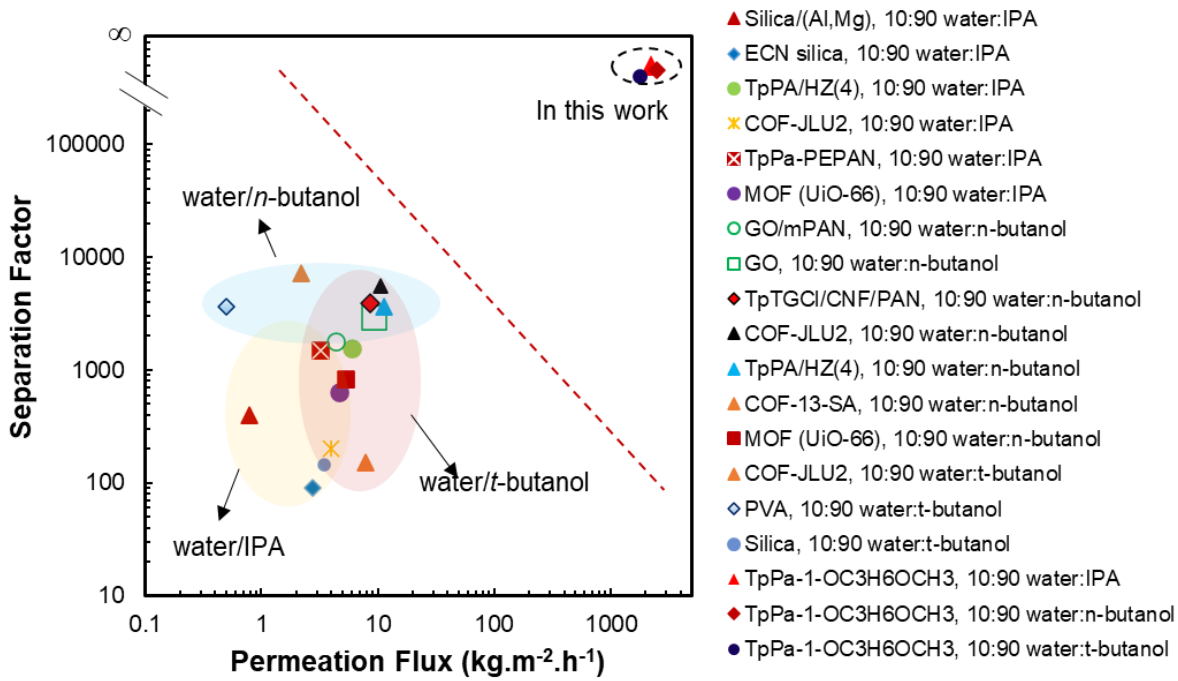

Fig. 8. Comparison of permeation flux and separation factor obtained from MD simulation against literature data available at 60-80 °C and 90 wt% alcohol mixture in water.

3.3 Activation energy (Ea)

It is important to estimate E_a for permeation for highly selective membrane, TpPa-1-OC3H6OCH3. As only water is permeated through this COF, only E_a for water is calculated for each mixture. As the feed temperature in PV increases from 320 K to 353 K, the permeation flux of water through TpPa-1-OC3H6OCH3 in water/IPA mixture also increased from 859.32 to 2219.9 kg/m^2.hr. For water/*n*-butanol and water/*t*-butanol mixtures, permeation fluxes increased from 787.7 to 2506.4 kg/m^2.hr and from 286.4 to 1790.3 kg/m^2.hr, respectively. As the feed temperature increases permeation fluxes increase, this could be due to: 1) increase in the partial pressure on the upstream side of the membrane as the feed temperature increases, enhancing mass transfer through the membrane[56] and 2) increase in the molecular transport rate as a result of greater thermal motion.[57] Water transport in a membrane generally follows the Arrhenius equation

$$J \sim \exp\left(\frac{-E_a}{RT}\right) \quad (3)$$

where E_a, R, and T are activation energy, gas constant, and temperature, respectively. To estimate E_a of water in TpPa-1-OC3H6OCH3, *ln* (*J*) versus (1000/T) were plotted in **Figure 9a**. The estimated E_a of water permeation for water/IPA, water/*n*-butanol and water/*t*-butanol mixtures are 24.88, 33.38, and 51.89 kJ/mol, respectively (**Figure 9b)**. The E_a of water for the highly selective membrane in water/IPA mixture is lower than the recently suggested COF-based membrane (35.81 kJ/mol).[20] Also, E_a of water in water/*n*-butanol mixture is close to COF-based membrane (31.38 kJ/mol)[53]. The E_a values increase in the order of E_a (water/IPA) < E_a (water/*n*-butanol) < E_a (water/*t*-butanol). To understand further the E_a trend, interaction energies (IE) between alcohols and water in mixtures are calculated. The hierarchy of IE is water/IPA (-20.8 kJ/mol) < water/*n*-butanol (-24.6 kJ/mol) < water/*t*-butanol (-26.2 kJ/mol). As water interacts strongly with *t*-butanol compared to *n*-butanol and IPA, they are expected to permeate slowly, thus leads to higher E_a. On the other hand, lesser interaction of water with IPA shows lower E_a.

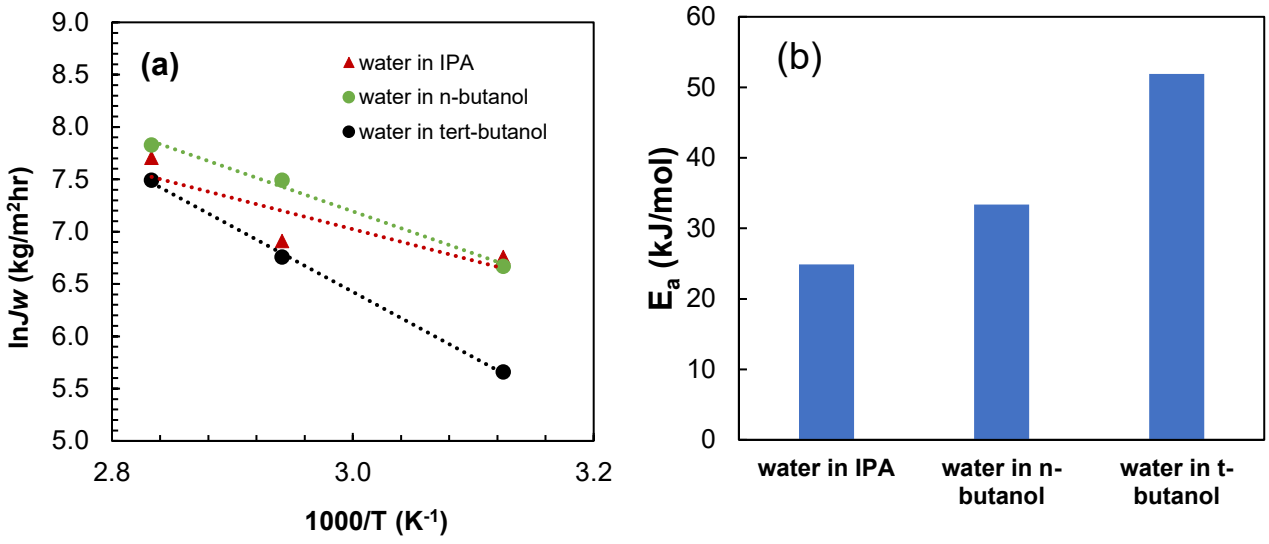

Fig. 9. (a) Flux through TpPa-1-OC3H6OCH3 membrane at various temperature by MD simulation. The dashed lines fit to the Arrhenius equation, and (b) activation of energy of water in mixture.

3.4 Characterization and experimental evaluation of sorption behaviour of COFs

After MD simulation, the parent and best-performing COF were experimentally synthesized. FT-IR analysis of the COF powders confirmed the expected chemical structure (**Fig. 10**). Absence of C=O

stretching frequency at 1640 cm^{-1} and carbonyl C-H stretching around 2880 cm^{-1} indicate the completion of condensation of Tp with 1,4-phenyline diamine ligand and formation of Schiff bases. This also results in the formation of a new C-N bond stretching vibration peak at 1257 cm^{-1} for TpPa-1 and 1251 cm^{-1} for TpPa-1-OC3H6OCH3 and C=C stretching vibration peak at 1580 cm^{-1} for TpPa-1 and 1577 cm^{-1} for TpPa-1-OC3H6OCH3, suggesting the irreversible tautomerism and confirming the presence of keto form.[45]

Both the COF powders appeared to be microcrystalline under polarized light microscopy. However, our extensive trials to grow bigger crystals failed to yield crystals suitable for single crystal X-ray diffraction. Therefore, crystallinity of the powders was gauged by PXRD. Both COFs exhibited close similarity in the PXRD patterns showing two intense peaks at lower 2θ values ($2\theta < 5°$), multiple broad peaks at higher 2θ values, and confirm the partial crystallinity of the powders (**Fig. 11**). The similarity of PXRD patterns suggests a similar structural features for the COFs. In this case, both the COFs could adopt a 2D sheet like structure. Microscopic analysis by SEM also confirmed the plate like morphology of TpPa-1-OC3H6OCH3 powders and ascertain the 2D sheet like structure (**Fig. 12**). PXRD patterns of the TpPa-1 and TpPa-1-OC3H6OCH3 were also generated using VASP optimised COF structures in Materials Studio and compared with experimental patterns (**Figure S3, Supporting Information**).

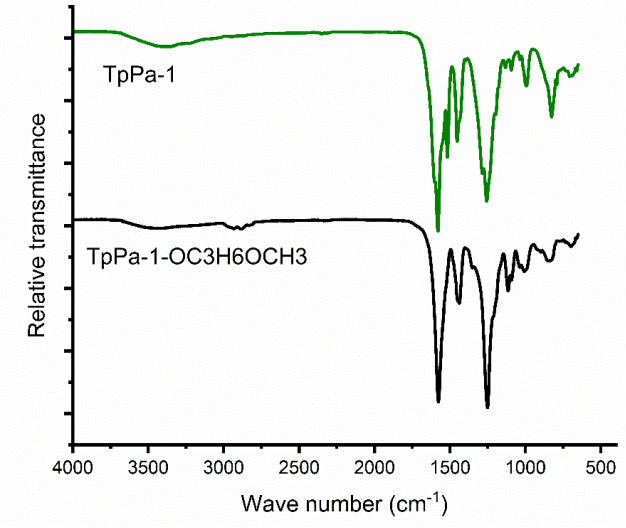

Fig. 10. Comparison of the FT-IR spectrum of TpPa-1 and TpPa-1-OC3H6OCH3.

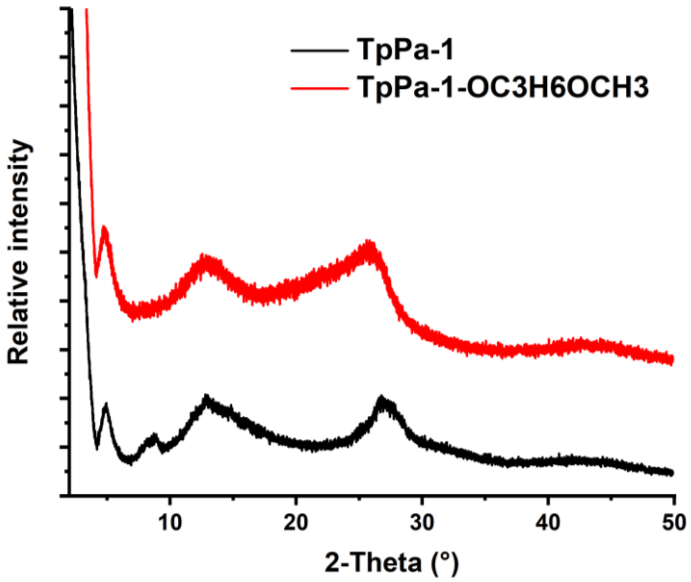

Fig. 11. PXRD patterns of TpPa-1 (black) and TpPa-1-OC3H6OCH3 (red) confirming the partial crystallinity of the powders.

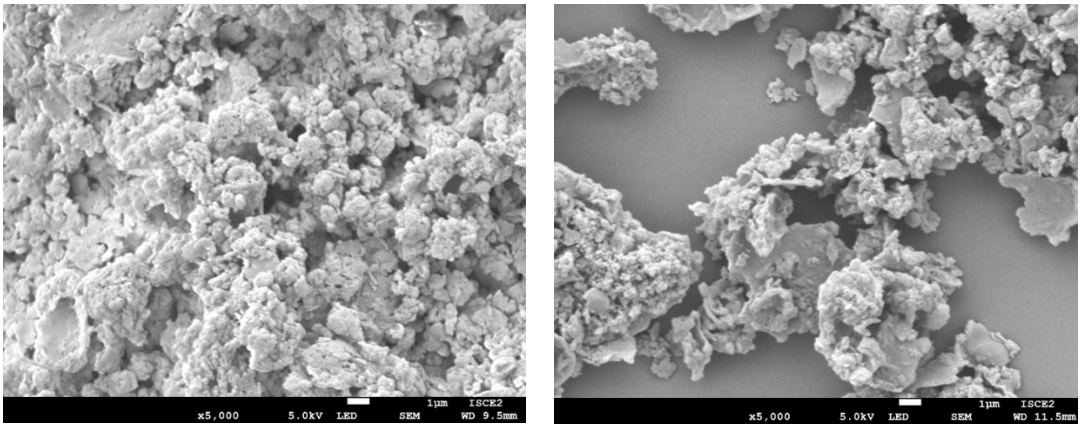

Fig. 12. SEM images of the COF powders, TpPa-1 (left) and TpPa-1-OC3H6OCH3 (right).

The adsorption capacity of the COFs, TpPa-1 and TpPa-1-OC3H6OCH3, was measured by BET N_2 adsorption and desorption curves. Both COFs showed reversible Type I adsorption isotherms which is characteristic of microporous structure (**Figure S4, Supporting Information**). The BET surface area of TpPa-1 is 523.2 m^2 g^{-1} which is similar to the surface area reported previously.[45] TpPa-1-OC3H6OCH3, on the other hand, showed lower BET surface area (28.3 m^2 g^{-1}) which is reminiscent of the small pores due to bulky -OC3H6OCH3 groups occupying the pores of TpPa-1 (**Figure S5-6**, **Supporting Information**). Similarly, TpPa-1 also showed higher Langmuir surface area than the

TpPa-1-OC3H6OCH3 (714.7 3 m^2 g^{-1} vs 40.1 3 m^2 g^{-1}). The calculated peak maxima from pore size distribution is 3.9 nm for TpPa-1 and 2.5 nm for TpPa-1-OC3H6OCH3 (**Figure S7, Supporting Information**). The smaller pores of the TpPa-1-OC3H6OCH3 suggests potential applications in the separation of solvents of smaller molecular dimension.

Separation of solvent mixtures through PV is generally explained by the solution-diffusion model which suggests that the solvent transport across the membrane of interest depends on three critical factors: sorption of solvent molecules on the membrane surface at the feed side, diffusion of solvent molecules through the membrane via concentration gradient, and desorption of solvent molecules from the membrane at the permeate side.[6, 24] While these factors affect the performance of a membrane and preferential separation of one solvent over the other, sorption of solvent molecules by the membrane plays the first and foremost mode of contact with the membrane. Generally, sorption of solvent molecules by a membrane is measured either by immersion of the membrane into the liquid (direct) or by contact with the vapor phase of the liquid (isopiestically).[58] Sorption of solvent molecules in the latter method occurs in the vapor phase, therefore the data that can be obtained from this method represents the sorption behaviour during PV. In this regard, the use of dynamic vapor sorption (DVS) technique draws prominence and can effectively be used to quantitatively measure the moisture sorption.[59] Recent advancements facilitated its use for studying organic vapor sorption phenomenon and allowed the determination of sorption, solvate formation, amorphous content, porosity, and surface energetics.[60] In the current work, the sorption behaviour of the COFs (TpPa-1 and TpPa-1-OC3H6OCH3) was studied using DVS technique by equilibrating the COF powders at different relative vapor pressure of water, IPA, *n*-butanol and *t*-butanol. It is well known that the sorption of moisture/solvent depends on the total surface area available for the solvent (or water) to interact with. In the case of materials with considerably larger pores, the ability of the solvents of appropriate size to interact with the pore walls also contribute to the overall sorption. As discussed before, TpPa-1 has 18-times higher (523.2 m^2 g^{-1}) BET surface area than the TpPa-1-OC3H6OCH3 (28.3 m^2 g^{-1}) which

is indicative of the larger pores in TpPa-1. **Fig. 13** shows the vapor sorption isotherms of TpPa-1 and TpPa-1-$OC_3H_6OCH_3$ with the solvents, water, IPA, *n*-butanol and *t*-butanol. It is evident that the COFs show distinct sorption behavior with TpPa-1 showing greater sorption than TpPa-1-OC3H6OCH3 with all the solvents tested. Interestingly, TpPa-1-OC3H6OCH3 showed lower sorption even though it features polar functional groups (-3-methoxypropoxy) and is more hydrophilic in nature than the TpPa-1.[61] This could be reasoned to the inability of the solvent molecules to enter the relatively small pores (**Figure S8, Supporting Information**). The PV MD simulation also confirms that solvent molecules are unable to penetrate the small pores of TpPa-1-OC3H6OCH3. Furthermore, the desorption isotherm confirms the near complete removal of the surface-adsorbed solvent molecules attesting the significant role of pore characteristics in the sorption and PV of solvents by the COFs. In the case of TpPa-1, the presence of larger pores enables passage of solvent molecules through the pores and get adsorbed not only on the surface, but also in the interstitial sites or the pores. It is also observed that not all the solvent molecules that are adsorbed by the TpPa-1 are removed during the desorption as it is possible that the solvents of relatively larger size (e.g. IPA, *n*-butanol and *t*-butanol) can be entrapped in the pores and are not possible to escape under the pressure conditions of the DVS. On the other hand, being smaller in molecular dimension, all the water molecules adsorbed by both TpPa-1 and TpPa-1-OC3H6OCH3 are completely removed during the desorption. The results of DVS experiments confirmed that both the COFs adsorbed the tested solvents including water. However, it is the pore size that determined the degree of sorption and retention of solvent molecules in the COF-pores. These observations aligned well with the computational results and highlight the value of integrating such methods to gain a deeper understanding of the solvent separation via PV. The DVS data also indicate that within the studied pressure range, solvents sorption increases in the order of *n*-butanol > IPA > *t*-butanol, reflecting the same order of sorption for associated water if they are in the mixture form, hence fluxes would also follow the same order. This is consistent with the hierarchy of the total fluxes [$J_{t(n\text{-butanol})} > J_{t(\text{IPA})} > J_{t(t\text{-butanol})}$] obtained by the MD simulation for TpPa-1-OC3H6OCH3.

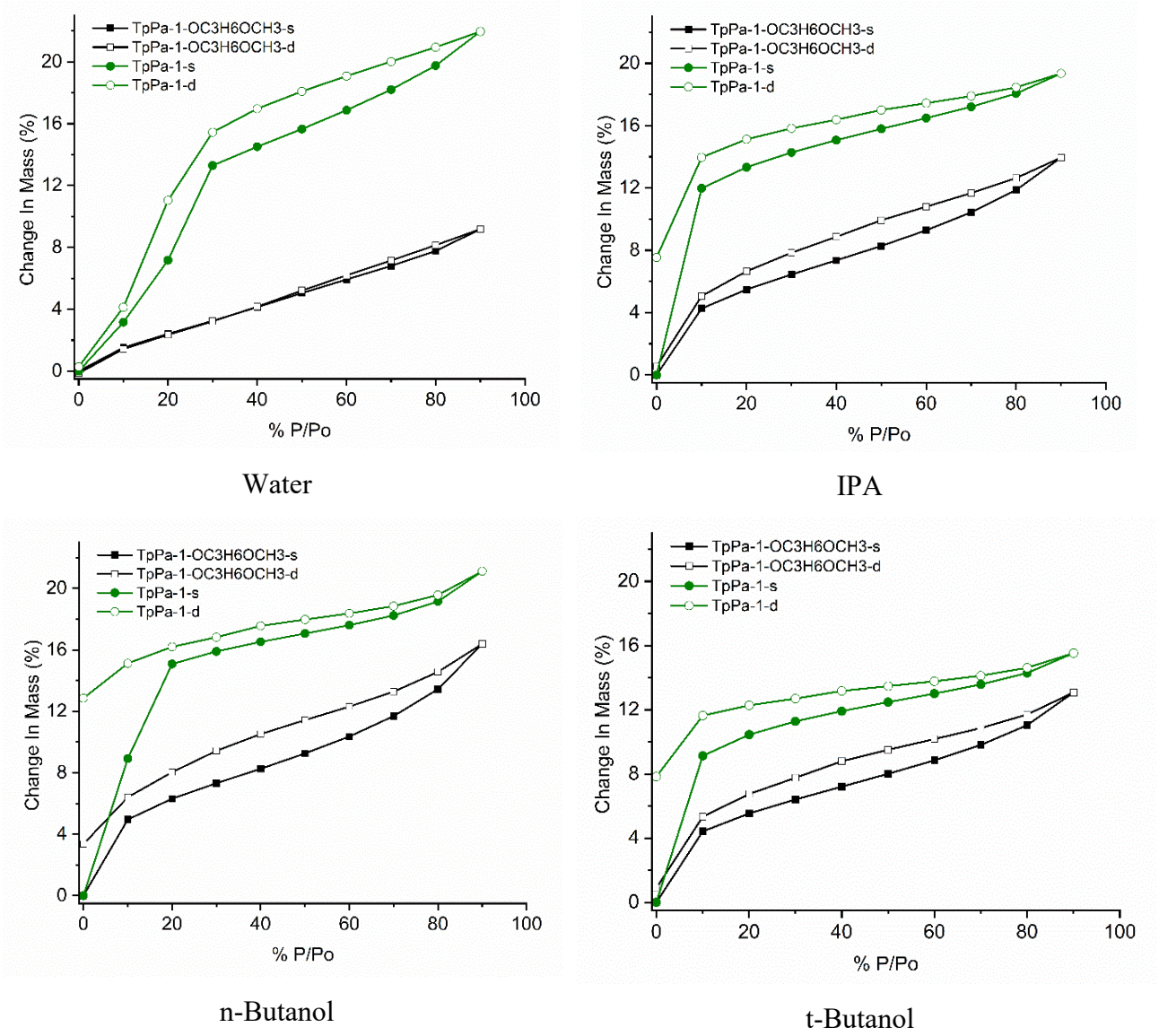

Fig. 13. Vapor sorption isotherms of TpPa-1 and TpPa-1-OC3H6OCH3 using water, and the solvents studied in this work from DVS experiments.

4. CONCLUSIONS

Various COF membranes were explored for alcohol dehydration (IPA, *n*-butanol and *t*-butanol) and a novel COF was designed. TpPa-1 was utilized as a model COF and its framework was modified via grafting new linker to develop novel COF. The hierarchy of permeation fluxes for solvent is TpPa-1-OC3H6OH < TpPa-1-C2Ph < TpPa-1-OC3H6OH < TpPa-1-COOC2H5 < TpPa-1-C5H8 < TpPa-1.

For all three alcohol mixtures, the permeation flux is mostly governed by the d_a. The largest d_a holds the highest flux whereas the smallest d_a leads to the lowest flux. In contrast, polarity of the pores and d_a both play critical role in determining the separation factor. The membranes with hydrophobic pore characteristics (TpPa-1-C5H8, TpPa-1-COOC2H5 and TpPa-1-C2Ph) display a lower separation factor than the membrane with hydrophilic pore (TpPa-1-OC3H6OH). The best-performing novel COF (TpPa-1-OC3H6OCH3) shows superior performance compared to the previously reported membranes. The E_a of water in alcohol mixtures through the TpPa-1-OC3H6OCH3 increases in the order of E_a (water/IPA) < E_a (water/*n*-butanol) < E_a (water/*t*-butanol). This is governed by water-alcohol interactions as the interaction energy increases in the order of water/IPA (-20.8 kJ/mol) < water/*n*-butanol (-24.6 kJ/mol) < water/*t*-butanol (-26.2 kJ/mol). The experimental sorption and desorption data were consistent with the MD simulation results. The TpPa-1 COF, with its larger pores and greater surface area, exhibited higher sorption capacity compared to TpPa-1-OC3H6OCH3, which allows solvent molecules to enter its relatively small pores. This study underscores the significance of integrating MD simulations with experimental tools for a comprehensive understanding of the application of COF for solvent separation using PV. The TpPa-1-OC3H6OCH3, with its superior separation performance, is a promising material for developing an advanced membrane for sustainable solvent recovery applications.

Integrating MD simulations with experimental validation combines the strengths of both methods to design more efficient COFs for solvent recovery. As demonstrated through our work, MD simulations offer atomic-level insights into COF structure, solvent interactions, and transport behaviour, guiding the design of novel COFs with optimized pore size and functionality. These simulations help predict solvent selectivity and recovery performance. Experimental techniques complement the MD simulations and validates the computational predictions under realistic conditions. Together, this hybrid approach facilitates the development of high-performance COFs tailored for effective solvent recovery.

It is worthwhile to note that, scalability is one of the primary challenges in the advancement of COFs towards commercialization and industrial applications. Oftentimes, synthesis of computationally designed COFs requires specific building blocks that involve multistep reactions and produce low yields. Furthermore, scale up of COFs can also lead to issues with uniformity, reproducibility, and poor crystallinity, which determine the performance of COF membranes.[62] While the recent advancements in the synthesis COFs holds great promise for developing efficient and scalable routes for their bulk synthesis,[63-66] the proposed integration of computational tools with experimental validation of COFs performance would reduce the burden of synthesizing a large number of building blocks for screening and selection of suitable COFs for effective solvent separation and recovery. In this regard, further research in improving the synthesis methods, optimizing membrane production techniques, and enhancing the performance of COFs in real-world applications, makes COF membranes a viable and sustainable solution for large-scale solvent recovery.

SUPPORTING INFORMATION

Supercell structure and 6-layer structure of TpPa-1-OC3H6OCH3; Functional groups, atomic notations and atomic charges TpPa-1-OC3H6OCH3; Force field parameters; Simulated PXRD spectra for TpPa-1 and TpPa-1-OC3H6OCH3 COFs; BET N_2 adsorption isotherm of TpPa-1 and TpPa-1-OC3H6OCH3; BET surface area plot for TpPa-1 and TpPa-1-OC3H6OCH3; Langmuir surface area plot for TpPa-1 and TpPa-1-OC3H6OCH3; Pore size distribution; pores of TpPa-1 and TpPa-1-OC3H6OCH3; PDB structural coordinates of TpPa-1 and TpPa-1-OC3H6OCH3.

AUTHOR INFORMATION

Corresponding Author

*** (K.M.G.) E-mail:** kmgchemical@gmail.com

AUTHOR ORCID ID's

1) Krishna M. Gupta: 0000-0003-4839-5980

2) Srinivasulu Aitipamula: 0000-0001-7640-9513
3) Xavier Chin
4) Pui Shan Chow: 0000-0002-5100-2677

Conflicts of interest

The authors declare no competing financial interest.

ACKNOWLEDGMENTS

This research is supported by the Agency for Science, Technology and Research (A*STAR) under its Career Development Fund (Project No. C210812028). This work was supported by the A*STAR Computational Resource Centre through the use of its high-performance computing facilities. We also acknowledge the National Supercomputing Centre of Singapore for providing computational resources for conducting part of the work. We thank NSJ Prayog Lifesciences Pvt Ltd., Hyderabad, India for their assistance with the synthesis of TpPa-1-OC3H6OCH3.

Reference:

1. Cseri, L.; Razali, M.; Pogany, P.; Szekely, G., Chapter 3.15 - Organic Solvents in Sustainable Synthesis and Engineering. In *Green Chemistry*, Török, B.; Dransfield, T., Eds. Elsevier: 2018; pp 513-553.
2. Constable, D. J. C.; Jimenez-Gonzalez, C.; Henderson, R. K., Perspective on Solvent Use in the Pharmaceutical Industry. *Organic Process Research & Development* **2007,** *11* (1), 133-137.
3. Solvent Use and Waste Issues. In *Green Chemistry in the Pharmaceutical Industry*, pp 49-82.
4. Vane, L. M., Review of pervaporation and vapor permeation process factors affecting the removal of water from industrial solvents. *Journal of Chemical Technology & Biotechnology* **2020,** *95* (3), 495-512.
5. Peng, P.; Lan, Y.; Liang, L.; Jia, K., Membranes for bioethanol production by pervaporation. *Biotechnology for Biofuels* **2021,** *14* (1), 10.
6. Liu, G.; Jin, W., Pervaporation membrane materials: Recent trends and perspectives. *J. Membr. Sci.* **2021,** *636*, 119557.
7. Ong, Y. K.; Shi, G. M.; Le, N. L.; Tang, Y. P.; Zuo, J.; Nunes, S. P.; Chung, T.-S., Recent membrane development for pervaporation processes. *Progress in Polymer Science* **2016,** *57*, 1-31.
8. Smitha, B.; Suhanya, D.; Sridhar, S.; Ramakrishna, M., Separation of organic–organic mixtures by pervaporation—a review. *Journal of Membrane Science* **2004,** *241* (1), 1-21.
9. Liang, B.; He, X.; Hou, J.; Li, L.; Tang, Z., Membrane Separation in Organic Liquid: Technologies, Achievements, and Opportunities. *Advanced Materials* **2019,** *31* (45), 1806090.
10. Shao, P.; Huang, R. Y. M., Polymeric membrane pervaporation. *Journal of Membrane Science* **2007,** *287* (2), 162-179.
11. Zhao, D.; Li, M.; Jia, M.; Zhou, S.; Zhao, Y.; Peng, W.; Xing, W., Asymmetric poly (vinyl alcohol)/Schiff base network framework hybrid pervaporation membranes for ethanol dehydration. *European Polymer Journal* **2022,** *162*, 110924.

12. Castro-Muñoz, R.; Buera-González, J.; Iglesia, Ó. d. l.; Galiano, F.; Fíla, V.; Malankowska, M.; Rubio, C.; Figoli, A.; Téllez, C.; Coronas, J., Towards the dehydration of ethanol using pervaporation cross-linked poly(vinyl alcohol)/graphene oxide membranes. *Journal of Membrane Science* **2019,** *582*, 423-434.
13. Selvaraj, M.; Banat, F., Ethanol-Water Separation Using Membrane Technology. In *Biorefinery: Integrated Sustainable Processes for Biomass Conversion to Biomaterials, Biofuels, and Fertilizers*, Bastidas-Oyanedel, J.-R.; Schmidt, J. E., Eds. Springer International Publishing: Cham, 2019; pp 211-232.
14. Bolto, B.; Hoang, M.; Xie, Z., A review of membrane selection for the dehydration of aqueous ethanol by pervaporation. *Chemical Engineering and Processing: Process Intensification* **2011,** *50* (3), 227-235.
15. Côté, A. P.; Benin, A. I.; Ockwig, N. W.; O'Keeffe, M.; Matzger, A. J.; Yaghi, O. M., Porous, Crystalline, Covalent Organic Frameworks. *Science* **2005,** *310* (5751), 1166-1170.
16. He, G.; Zhang, R.; Jiang, Z., Engineering Covalent Organic Framework Membranes. *Accounts of Materials Research* **2021,** *2* (8), 630-643.
17. Yang, H.; Yang, L.; Wang, H.; Xu, Z.; Zhao, Y.; Luo, Y.; Nasir, N.; Song, Y.; Wu, H.; Pan, F.; Jiang, Z., Covalent organic framework membranes through a mixed-dimensional assembly for molecular separations. *Nature Communications* **2019,** *10* (1), 2101.
18. Yang, H.; Wu, H.; Yao, Z.; Shi, B.; Xu, Z.; Cheng, X.; Pan, F.; Liu, G.; Jiang, Z.; Cao, X., Functionally graded membranes from nanoporous covalent organic frameworks for highly selective water permeation. *Journal of Materials Chemistry A* **2018,** *6* (2), 583-591.
19. Zhang, Z.; Yang, H.; Cao, C.; Liu, Y.; Liang, S.; Wang, M.; Wang, H.; Cao, X.; Pan, F.; Wu, H.; Jiang, Z., Vapor-liquid interfacial polymerization of covalent organic framework membranes for efficient alcohol dehydration. *Journal of Membrane Science* **2022,** *641*, 119905.
20. Wang, X.; Wang, N.; Ni, H.; Liu, T.; An, Q.-F., Oxygen plasma-assisted contra-diffusion self-assembly of covalent organic framework pervaporation membranes for organic-solvent dehydration. *Journal of Membrane Science* **2023,** *665*, 121129.
21. Yuan, J.; Zheng, J.; Zhou, C.; Cao, J.; Wang, Z.; Jin, Y.; Zhang, S.; Zhang, Z.; Zhou, P.; Chen, X.; Shen, H.; Liu, G.; Jin, W., Incorporating covalent organic framework nanosheets via solvent-exchange strategy boosted hybrid membrane dehydration performance. *Separation and Purification Technology* **2025,** *353*, 128315.
22. Yuan, S.; Li, X.; Zhu, J.; Zhang, G.; Van Puyvelde, P.; Van der Bruggen, B., Covalent organic frameworks for membrane separation. *Chemical Society Reviews* **2019,** *48* (10), 2665-2681.
23. Jin, Y.-H.; Li, M.-H.; Yang, Y.-W., Covalent Organic Frameworks for Membrane Separation. *Advanced Science* **2025,** *12* (5), 2412600.
24. Wang, C.; Yan, X.; Liu, X., Polycrystalline Metal–Organic Framework Membranes for Pervaporation. *Industrial & Engineering Chemistry Research* **2023,** *62* (28), 10787-10799.
25. Gupta, K. M.; Aitipamula, S.; Chow, P. S., In-silico design of covalent organic framework membranes for efficient water/ethanol separation. *J. Membr. Sci.* **2023,** *687*, 122083.
26. Biswal, B. P.; Kandambeth, S.; Chandra, S.; Shinde, D. B.; Bera, S.; Karak, S.; Garai, B.; Kharul, U. K.; Banerjee, R., Pore surface engineering in porous, chemically stable covalent organic frameworks for water adsorption. *Journal of Materials Chemistry A* **2015,** *3* (47), 23664-23669.
27. BIOVIA, Dassault Systèmes. Materials Studio, San Diego, 2021.
28. Kresse, G.; Hafner, J., Ab initio molecular dynamics for liquid metals. *Physical review B* **1993,** *47* (1), 558.
29. Kresse, G.; Hafner, J., Ab initio molecular-dynamics simulation of the liquid-metal--amorphous-semiconductor transition in germanium. *Physical Review B* **1994,** *49* (20), 14251-14269.
30. Kresse, G.; Furthmüller, J., Efficient iterative schemes for ab initio total-energy calculations using a plane-wave basis set. *Physical Review B* **1996,** *54* (16), 11169-11186.
31. Hafner, J., Ab-initio simulations of materials using VASP: Density-functional theory and beyond. *Journal of Computational Chemistry* **2008,** *29* (13), 2044-2078.

32. Willems, T. F.; Rycroft, C. H.; Kazi, M.; Meza, J. C.; Haranczyk, M., Algorithms and tools for high-throughput geometry-based analysis of crystalline porous materials. *Microporous and Mesoporous Materials* **2012,** *149* (1), 134-141.
33. Gupta, K. M.; Liu, J.; Jiang, J., A molecular simulation protocol for membrane pervaporation. *Journal of Membrane Science* **2019,** *572*, 676-682.
34. Manz, T. A.; Sholl, D. S., Chemically Meaningful Atomic Charges That Reproduce the Electrostatic Potential in Periodic and Nonperiodic Materials. *Journal of Chemical Theory and Computation* **2010,** *6* (8), 2455-2468.
35. Rappe, A. K.; Casewit, C. J.; Colwell, K. S.; Goddard, W. A., III; Skiff, W. M., UFF, a full periodic table force field for molecular mechanics and molecular dynamics simulations. *Journal of the American Chemical Society* **1992,** *114* (25), 10024-10035.
36. Zhang, Y.; Fang, T.; Hou, Q.; Li, Z.; Yan, Y., Water desalination of a new three-dimensional covalent organic framework: a molecular dynamics simulation study. *Physical Chemistry Chemical Physics* **2020,** *22* (29), 16978-16984.
37. Shi, Q.; He, Z.; Gupta, K. M.; Wang, Y.; Lu, R., Efficient ethanol/water separation via functionalized nanoporous graphene membranes: insights from molecular dynamics study. *Journal of Materials Science* **2017,** *52* (1), 173-184.
38. Liu, J.; Li, L.; Zhao, Z.; Yu, F., Porous Organic Cage Membranes for Biofuel Purification via Pervaporation: A Molecular Simulation Study. *ACS Sustainable Chemistry & Engineering* **2021,** *9* (44), 14890-14899.
39. Wang, M.; Jiang, J., Multilayered graphene oxide membranes for bioethanol purification: Microscopic insight from molecular simulation. *Journal of Membrane Science* **2022,** *660*, 120888.
40. Jorgensen, W. L.; Maxwell, D. S.; Tirado-Rives, J., Development and Testing of the OPLS All-Atom Force Field on Conformational Energetics and Properties of Organic Liquids. *J. Am. Chem. Soc.* **1996,** *118*, 11225-11236.
41. Gupta, K. M.; Liu, J.; Jiang, J., A molecular simulation study for efficient separation of 2,5-furandiyldimethanamine by a microporous polyarylate membrane. *Polymer* **2019,** *175*, 8-14.
42. Ribeiro, A. A.; Horta, B. A.; Alencastro, R. B. d., MKTOP: a program for automatic construction of molecular topologies. *Journal of the Brazilian Chemical Society* **2008,** *19* (7), 1433-1435.
43. Jorgensen, W. L.; Chandrasekhar, J.; Madura, J. D.; Impey, R. W.; Klein, M. L., Comparison of Simple Potential Functions for Simulating Liquid Water. *J. Chem. Phys.* **1983,** *79* (2), 926-935.
44. Hess, B.; Kutzner, C.; van der Spoel, D.; Lindahl, E., GROMACS 4: Algorithms for highly efficient, load-balanced, and scalable molecular simulation. *J. Chem. Theory Comput.* **2008,** *4* (3), 435-447.
45. Kandambeth, S.; Mallick, A.; Lukose, B.; Mane, M. V.; Heine, T.; Banerjee, R., Construction of Crystalline 2D Covalent Organic Frameworks with Remarkable Chemical (Acid/Base) Stability via a Combined Reversible and Irreversible Route. *Journal of the American Chemical Society* **2012,** *134* (48), 19524-19527.
46. NSJ Prayog Life Sciences Pvt Ltd., Hyderabad, India. https://www.prayoglife.com/.
47. Zhang, K.; Gupta, K. M.; Chen, Y.; Jiang, J., Biofuel purification in GME zeolitic–imidazolate frameworks: From ab initio calculations to molecular simulations. *AIChE Journal* **2015,** *61* (9), 2763-2775.
48. Gupta, K. M.; Qiao, Z.; Zhang, K.; Jiang, J., Seawater Pervaporation through Zeolitic Imidazolate Framework Membranes: Atomistic Simulation Study. *ACS Applied Materials & Interfaces* **2016,** *8* (21), 13392-13399.
49. Gupta, K. M.; Shi, Q.; Sarkisov, L.; Jiang, J., Ethanolamine Purification by Nanofiltration through PIM-1 and Carbon Membranes: A Molecular Simulation Study. *The Journal of Physical Chemistry C* **2017,** *121* (37), 20539-20545.
50. Borjigin, T.; Sun, F.; Zhang, J.; Cai, K.; Ren, H.; Zhu, G., A microporous metal–organic framework with high stability for GC separation of alcohols from water. *Chemical Communications* **2012,** *48* (61), 7613-7615.
51. Cao, Y.; Wang, K.; Wang, X.; Gu, Z.; Gibbons, W.; Vu, H., Adsorption of butanol vapor on active carbons with nitric acid hydrothermal modification. *Bioresource Technology* **2015,** *196*, 525-532.

52. Liu, X.; Wang, C.; Wang, B.; Li, K., Novel Organic-Dehydration Membranes Prepared from Zirconium Metal-Organic Frameworks. *Advanced Functional Materials* **2017,** *27* (3), 1604311.
53. Cao, C.; Wang, H.; Wang, M.; Liu, Y.; Zhang, Z.; Liang, S.; Yuhan, W.; Pan, F.; Jiang, Z., Conferring efficient alcohol dehydration to covalent organic framework membranes via post-synthetic linker exchange. *Journal of Membrane Science* **2021,** *630*, 119319.
54. Wang, H.; Chen, L.; Yang, H.; Wang, M.; Yang, L.; Du, H.; Cao, C.; Ren, Y.; Wu, Y.; Pan, F.; Jiang, Z., Brønsted acid mediated covalent organic framework membranes for efficient molecular separation. *Journal of Materials Chemistry A* **2019,** *7* (35), 20317-20324.
55. Gallego-Lizon, T.; Edwards, E.; Lobiundo, G.; Freitas dos Santos, L., Dehydration of water/t-butanol mixtures by pervaporation: comparative study of commercially available polymeric, microporous silica and zeolite membranes. *Journal of Membrane Science* **2002,** *197* (1), 309-319.
56. Teli, S. B.; Gokavi, G. S.; Sairam, M.; Aminabhavi, T. M., Highly water selective silicotungstic acid (H4SiW12O40) incorporated novel sodium alginate hybrid composite membranes for pervaporation dehydration of acetic acid. *Separation and Purification Technology* **2007,** *54* (2), 178-186.
57. Svang-Ariyaskul, A.; Huang, R. Y. M.; Douglas, P. L.; Pal, R.; Feng, X.; Chen, P.; Liu, L., Blended chitosan and polyvinyl alcohol membranes for the pervaporation dehydration of isopropanol. *Journal of Membrane Science* **2006,** *280* (1), 815-823.
58. Freger, V.; Korin, E.; Wisniak, J.; Korngold, E., Measurement of sorption in hydrophilic pervaporation: sorption modes and consistency of the data. *Journal of Membrane Science* **2000,** *164* (1), 251-256.
59. Shafiur Rahman, M.; Hamed Al-Belushi, R., Dynamic Isopiestic Method (DIM): Measuring Moisture Sorption Isotherm of Freeze-Dried Garlic Powder and Other Potential Uses of DIM. *International Journal of Food Properties* **2006,** *9* (3), 421-437.
60. Kaur, A.; Kale, D. P.; Bansal, A. K., Surface characterization of pharmaceutical solids. *TrAC Trends in Analytical Chemistry* **2021,** *138*, 116228.
61. Mahajan, J. S.; Shokrollahzadeh Behbahani, H.; Green, M. D.; Korley, L. T. J.; Epps, T. H., Increased hydrophilicity of lignin-derivable vs. bisphenol-based polysulfones for potential water filtration applications. *RSC Sustainability* **2024,** *2* (10), 2844-2850.
62. Vardhan, H.; Rummer, G.; Deng, A.; Ma, S., Large-Scale Synthesis of Covalent Organic Frameworks: Challenges and Opportunities. *Membranes* **2023,** *13* (8), 696.
63. Guo, L.; Zhang, Q. Y.; Yu, Z.; Krishna, R.; Luo, F., Minute and Large-Scale Synthesis of Covalent-Organic Frameworks in Water at Room Temperature by a Two-Step Dissolution–Precipitation Method. *Chem. Mater.* **2023,** *35* (14), 5648-5656.
64. Wu, D.; Gu, N.; Yao, J.; Cao, Y.; Wang, L.; Shakir, I.; Sun, Y.; Xu, Y., Recent advances in room-temperature synthesis of covalent organic frameworks. *Chem Sci* **2025,** *16* (13), 5447-5463.
65. Qing, Q.; Luo, J.; Liu, S.; Wang, J.; Wang, Z.; Xiong, X.-G.; Chen, J.; Lu, Y., General synthesis of covalent organic frameworks under ambient condition within minutes via microplasma electrochemistry approach. *Nature Communications* **2025,** *16* (1), 2571.
66. Åhlén, M.; Kong, X.; Zhao, W.; Zamora, F.; Xu, C., Overcoming Boundaries: Towards the Ambient Aqueous Synthesis of Covalent Organic Frameworks. *Angew. Chem. Int. Ed.* **2025,** *64* (15), e202425426.